Journal of Energy Storage 52 (2022) 104844

Contents lists available at ScienceDirect

Journal of Energy Storage

journal homepage: www.elsevier.com/locate/est

Research Papers

Modeling and total cost optimization of battery thermal management system in a hybrid electric vehicle

Ali Asef [a,c], Iman Chitsaz [b,*], Navid Madani [c]

[a] Department of Mechanical Engineering, Faculty of Engineering, Golestan University, Gorgan, Iran
[b] Department of Mechanical Engineering, Isfahan University of Technology, Isfahan 84156-83111, Iran
[c] Irankhodro Powertrain Co. (IP-CO), Tehran 1398813711, Iran

ARTICLE INFO

Keywords:
Battery thermal management
Optimization
Heat generation model
Hybrid electric vehicle
Total cost of ownership

ABSTRACT

In the present study, the battery thermal management of a series hybrid electric vehicle is modeled and optimized for different standard driving conditions. The heat generation of the battery is comprehensively studied in previous works for the steady-state charge or discharge of the battery. Despite the previous investigations, the heat generation of the battery in the present study is modeled for the real driving conditions in terms of battery state of charge and power consumption. The model is validated with the experimental data. The validated model is implemented to minimize the total cost of ownership of the battery thermal management system. In this way, the battery thermal management system is optimized for three different standard driving cycles. The independent variables are the compressor speed, fan speed, chiller size, radiator size, and condenser size. The results reveal that the total cost of optimization is converged to 200 US dollars for all driving cycles. The optimum configuration of the battery thermal management system does not considerably vary for different driving cycles. Therefore, one of the optimum configurations can be considered the overall optimum for battery thermal management.

1. Introduction

The automotive industry is shifting to electric [1] and hybrid electric vehicles [2] due to the environmental issues of conventional internal combustion engine vehicles, fossil fuels, strict emission laws [3], encouraging policies [4], and improvement in high-efficiency batteries [5]. The biggest hurdle in developing HEVs and EVs is energy storage [6,7]. Li-ion batteries are employed in electrified vehicles due to the long life cycle, high energy capacity, and energy density. The operating temperature considerably affects the high voltage batteries' life, safety, and performance. The appropriate operating temperature range for batteries is 15– to 35 °C [8]. Therefore, cooling, heating, ventilating, and insulating the batteries is necessary to achieve the desired operating temperature. Different BTMS configurations are proposed by researchers [8]. Air-cooled, liquid-cooled, PCM type, heat pipe type [9], and thermoelectric type are different categories of BTMS. From another perspective, BTMS can be clustered into passive, active, and hybrid systems. The passive system normally utilizes PCM [10–12], heat pipe [13], or air convection that consumes minimum power. Hybrid systems implement both advantages of passive and active systems. Air-cooled systems usually are less expensive and more complicated than other BTMS configurations. This type is implemented in vehicles with low cooling demand for batteries [14]. On the other hand, active liquid-based systems are the most popular BTMS configuration in the automotive industry. Refrigerant and heaters are implemented in the coolant circuit to accommodate the battery operating requirement in warm and cold climate conditions [15]. Notably, these systems consume more energy than the passive BTMS.

Some researchers focused on the efficiency improvement of the battery cooling systems. In this regard, Tang et al. [16] proposed a coupling system of liquid-cooled BTMS and heat pump air conditioning system for battery electric vehicles. The cooling capacity and system COP for their model were improved compared to the previous models. Kuang et al. [17] designed a BTMS and implemented a control strategy for compressor speed considering battery lifetime. According to the simulated results, the phased control method consumed 10.7% less energy than the standard constant compressor speed control method with the same situations. Tian et al. [18] proposed an electric vehicle thermal management system with waste heat recovery from the motor and controller unit that could save 162.3–249.44 € per year operating costs. EVTMS had a payback period ranging from 4.57 to 6.77 years. It has

* Corresponding author.
E-mail addresses: a_asef@ip-co.com (A. Asef), i.chitsaz@iut.ac.ir (I. Chitsaz), n_madani@ip-co.com (N. Madani).

https://doi.org/10.1016/j.est.2022.104844
Received 21 February 2022; Received in revised form 2 May 2022; Accepted 7 May 2022
Available online 13 May 2022

Nomenclature

1D	one dimensional
Amb	Ambient
BEV	battery electric vehicle
BTMS	battery thermal management system
C	rate at which a battery is being charged or discharged
COP	Coefficient of performance
EV	electric vehicle
EVTMS	electric vehicle thermal management system
FTP	federal test procedure
HEV	hybrid electric vehicle
HGP	heat generation percentage
HPACS	heat pump air conditioning system
Hys	hysteresis
HX	heat exchanger
ICEVs	internal combustion engine vehicles
NEDC	New European Driving Cycle
PCM	phase change material
SOC	state of charge
TCO	total cost of ownership
TMS	thermal management strategy, thermal management system
TXV	thermal expansion valve
VCU	vehicle control unit
WLTC	worldwide harmonized light vehicles test cycle

Symbols

A	area, m^2
C_p	heat capacity of the wall, kJ/ (m^2. K)
c_f	fanning friction factor
D	equivalent diameter, m
d	tube thickness, m
dp	pressure differential acting across dx
dx	length of mass element in the flow direction
e	total internal energy, kJ/kg
H	total specific enthalpy, $H = e + \frac{p}{\rho}$, kJ/kg
h	convective heat transfer coefficient, W/ (m^2. K)
i	interest rate
i	simulation time step,
K_p	pressure loss coefficient
k	thermal conductivity, W/ (m. K)
m	number of months
m	mass, kg
n	number of years
P	power, kW
Q	heat transfer rate, kW
Q_{gen}	battery heat generation, kW
Q_s	slave side heat transfer, kW
T	temperature, °C
T_{SH}	instant superheat temperature, °C
T_{target}	target superheat temperature, °C
t	time, s
$t_{simulation}$	duration of simulation, s
u	velocity at boundary, m/s
V	volume, m^3
$\dot{V}$	volume flow rate, m^3/s
V_D	volumetric displacement, lit
$\dot{m}$	mass flow rate, kg/s
η_v	volumetric efficiency
ΔT	temperature difference, °C
X	initial cost of components
Z	5-year fuel cost

Greek letters

γ	specific heat ratio,
ρ	density, kg/m^3

Subscripts

batt	battery
in	inlet
m	master
s	slave
S	surface

been suggested that increasing the amount of waste heat and lowering the condensation temperature can improve performance. Tian et al. [19] presented a thermal management system for electric vehicles, including cabin thermal comfort, battery cooling system, and motor waste heat recovery. The effects of compressor speed, environmental temperature, waste heat load, predicted energy consumption, system capacity, and COP were investigated in this study. They showed that the millage range of an electric vehicle could be increased by up to 31.71% employing the new electric vehicle thermal management system. A modern BTMS with an evaporator and a chiller was explored at various cooling temperatures by Alkhulaifi et al. [20]. They discovered that the ejector implementation has the advantage of increasing the compressor's inlet pressure while reducing power consumption. They showed that COP could be improved from 7.17 to 77.9% compared to the primary system. The refrigerant charge and the heat rejected by the condenser were decreased by 14% and 14.4%, respectively. Hamut et al. [21,22] studied the TMS of a range-extended EV. They investigated the vehicle's refrigerant and coolant circuits under extremely high temperatures, identifying exergy efficiencies and their impact on the overall system. Their research also included an exergy-based economic analysis of electrified automobiles. Wang et al. [23,24] optimized the air-cooled BTMS of a battery pack. The objectives were to maximize the battery life and minimize the battery volume, the fan's power, and the temperature difference among different cells. A combination of the heat pipe and refrigerant-based BTMS coupled with an air-conditioning system was investigated by Yao et al. [25]. The effects of ambient temperatures and battery heat generation rates were investigated on the battery temperature distribution, energy efficiency, and exergy efficiency of BTMS. Akinlabi and solyali [26] reviewed air-cooled BTMS techniques (passive and active) and designed parameter optimization methods for improving various BTMS design objectives. Fayaz et al. [27] also reviewed optimizing the battery packs' thermal and structural design parameters under different BTMSs. Liang et al. [28] investigated that intermittent cooling consumes less power than constant cooling in a heat pipe-based BTMS. A comparative investigation of key design factors and optimal architectures with a new battery electro-model performed by [29]. Surrogate-based optimization used to execute grouped-channel optimizations based on parametric analysis. Liquid cooling BTMS using serpentine microchannels studied by [30]. They investigated the entrance direction of serpentine microchannel cooling plates. The surrogate aided technique used to parameterize and simulate the problem. The multiobjective genetic algorithm (MOGA) was then implemented to optimize the serpentine channel, and water flow velocity parameters. A simple PCM cooling structure investigated by [31]. cooling behavior and the impact of numerous specific parameters on performance, such as PCM thickness, phase change temperature (PCT), and laying aside during dynamic cycling, analyzed. The experimental results reveal that a PCM module with a thickness of 10 mm provides the best cooling performance. A series of experiments with and without fins carried out by [32] to evaluate the impacts of different fin configurations. The

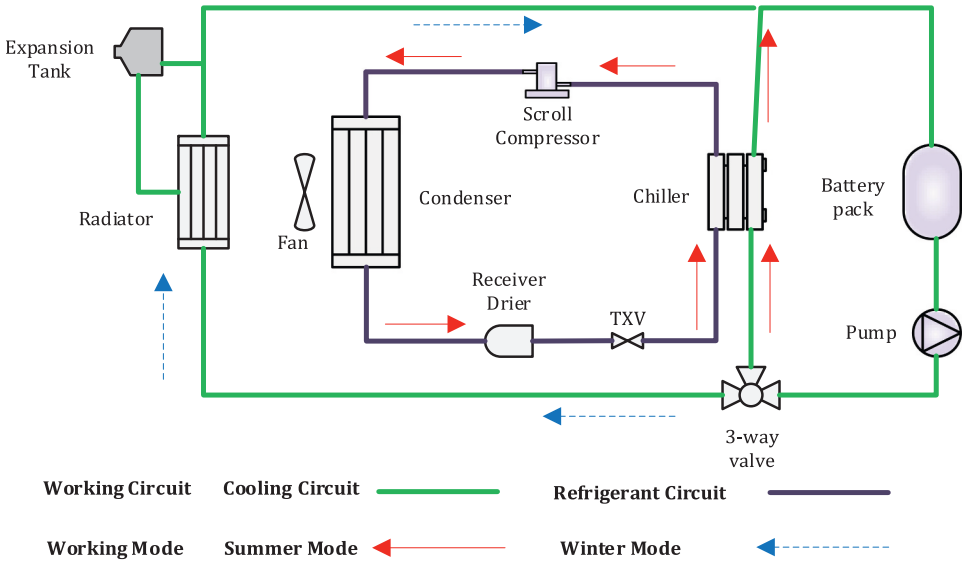

Fig. 1. Schematic of BTMS.

experimental results demonstrate that longitudinal fins are advantageous for heat dissipation at the bottom and air convection with the ambient, but circular fins have superior heat conduction due to their higher surface area.

The temperature gradient between the cells of the battery pack is investigated by many researchers. In this regard, Cen et al. [33] designed the thermal management module with a simple finned-tube heat exchanger structure and a customized aluminum frame. The temperature variations in the steady discharging rate of 0.5C, 1C, 1.5C in laboratory experiments was less than 4 °C. The temperature variations of the battery pack in road driving tests were reported at less than 1.5 °C. Chen et al. [34,35] optimized the spacings among the battery cells of the air-cooled battery pack. The cooling performance of the battery pack was improved in this study in which the maximum temperature difference was reduced by 42% with no significant effect on pressure drop. The structure of the BTMS is optimized by arranging the widths of the inlet divergence plenum and the outlet convergence plenum without changing the layout of the battery cells. Chen et al. [36] was also investigated the effects of geometrical dimensions of the battery pack on the temperature variations. They optimized the battery pack structure for a 5C discharge rate, and the temperature difference among the battery cells was reduced by 70% after optimization. Cheng et al. [37] optimized the air-cooled BTMS with the goal of the average battery temperature minimization, the standard deviation of battery temperature minimization, and the pressure drop minimization. Due to several goals, multiobjective optimization is implemented in their research. The BTMS of the air-cooled battery pack with the typical U-type cooling system was designed to optimize temperature uniformity by Shi et al. [38]. The artificial neural network was implemented to find the relationship between the pack's temperature and independent variables. The maximum temperature in their optimum design was decreased by 6.22 K compared to the original design.

BTMS control strategy is also thoroughly investigated by many researchers. A novel refrigerant-based BTMS was investigated by Shen et al. [39]. The system's temperature responsiveness, energy efficiency, and irreversibility effects were investigated. The entire vehicle thermal management system was optimized employing a cabin-prioritized control strategy. The air-cooled BTMS for the electric vehicle with a rule-based multiparameter control strategy was investigated by Fan et al. [40]. The trade-off between battery life and vehicle drive range was studied in this study. Hou et al. [41] optimized the air cooled BTMS based on field synergy equation. A comprehensive review on different cooling strategy of BTMS was also performed by Lu et al. [42].

Implementing the PCM is recently investigated for the battery cooling system by some researchers.

Javani et al. [43] implemented the octadecane as the PCM in the battery cooling system. Li et al. [44] implemented PCM to control the BTMS of the battery pack. The objective function was to minimize the mass of PCM. The expanded graphite (EG)/paraffin (PA) composite PCM was implemented in their study.

Although various studies have been conducted on BTMS efficiency improvement, there is still a gap in the literature to investigate simultaneously performance and cost that can be implemented in the automotive industry. Notably, a novel model for the heat generation of the battery pack is proposed in the present study. The literature's available battery heat generation models are limited to steady-state working conditions. The presented heat generation model considers transient driving conditions that is more applicable in real driving conditions. Implementing this novel model, the size of the thermal management system's components is optimized to minimize the total cost of vehicle ownership. The presented heat generation model is extracted by the real driving of the hybrid electric vehicle. Then, a numerical model is built based on the experimental data and validated with the experiments. The validated model is implemented to optimize the size of components. Three different driving cycles are implemented to investigate the effects of driving conditions on the size of components and the total cost of ownership.

2. Method and model

2.1. BTMS description

Battery thermal management system (BTMS) has a crucial role in the battery life cycle (BLC) and the energy consumption of hybrid electric vehicles (HEVs). In the present study, the BTMS model is created with comprehensive details of all components to investigate the effects of design parameters on the total customer ownership (TCO). The present study considers two separate coolant and refrigerant circuits that engage via a chiller. The schematic of investigated BTMS is shown in Fig. 1. This figure shows that the system consists of air-cooling and refrigerant cooling circuits that are activated in different conditions. The battery cooling system consists of a pump, battery block, 3-way solenoid valve, chiller coolant side, radiator coolant side, expansion tank, connecting pipes, and hoses. The refrigerant line consists of a chiller, scroll

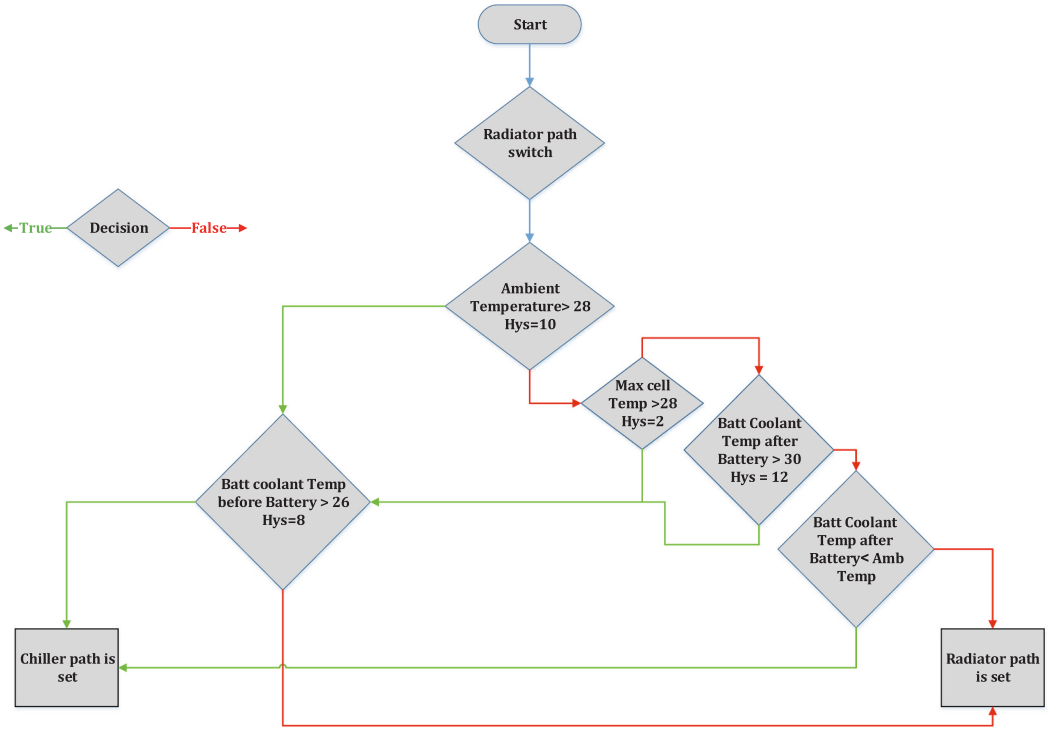

Fig. 2. Schematic of TMS.

Table 1
Heat exchanger master & slave fluid flow.

Heat exchanger	Master side	Slave side
Radiator	Coolant	Air
Condenser	Refrigerant	Air
Chiller	Refrigerant	Coolant

compressor, condenser, receiver drier, thermal expansion valve (TXV), and connecting pipes. The airflow passage is also considered to simulate airflow over the condenser and radiator. The airflow consists of a cooling fan, radiator airside, condenser airside, and connecting pipes. The coolant in the battery cooling system is ethylene glycol-water (with a volume fraction of 50%), and the refrigerant is R-134a.

The main target of an optimized BTMS is to achieve the appropriate conditions for the battery in different driving and weather conditions. The best temperature range for the battery cells is 16–28 °C. The present thermal management strategy (TMS) is shown in Fig. 2. As shown in this figure, the radiator path is the default passage for the cooling system to minimize the energy consumption of the BTMS. The first checking condition is the ambient temperature. If the ambient temperature is higher than the specified temperature(28 °C), the chiller passage will be active. At the second condition, the cell temperature of the battery is investigated. The chiller path is turned on at the high temperature of battery cells(28 °C).

Furthermore, the third condition is related to the coolant temperature at the exit of the battery. If the exit temperature of the coolant is more than the specified value(30 °C), the heat rejection needs to be improved. Therefore, the chiller path will be active in this condition. At the final step, the coolant temperature after the battery is compared with the ambient temperature. If the ambient temperature is more than the coolant temperature after the battery, the coolant is directed to the chiller path to preserve its temperature and save energy. Notably, conditions 1 to 3 should be checked with one additional condition. This condition is related to the coolant temperature before the battery. If this temperature is reduced too much, the energy consumption is increased. In this condition, the radiator path will be active. These conditions are assigned to preserve the battery coolant temperature in the range of 15 to 30 °C. Therefore, the operating temperature of battery cells is preserved in the range of 15– to 35 °C by these conditions.

2.2. Governing equations

In the present study, the commercial GT-SUITE software is implemented to optimize the BTMS performance for the proposed TMS. The following assumptions are considered in the simulations as follow:

1. Initial conditions are in equilibrium with the surrounding medium.
2. The electric pump is not considered due to its low power consumption compared to the other components.
3.The air conditioning system of the cabin is not considered in the present study.

The flow model involves the solution of the Navier-Stokes equations, namely the conservation of continuity and momentum. Energy equations are also solved simultaneously. These equations are solved in one dimension, which means that all quantities are averages across the flow direction. Mass flow, density, and internal energy are solved by the explicit method, while the implicit procedure uses pressure and total enthalpy. One dimensional governing equations are solved by GT-SUITE for explicit solver as follows [45]:

Continuity:

$$\frac{dm}{dt} = \sum \dot{m} \tag{1}$$

Energy:

$$\frac{d(me)}{dt} = -p\frac{dV}{dt} + \sum(\dot{m}H) - hA_S\left(T_{fluid} - T_{wall}\right) \tag{2}$$

Momentum:

$$\frac{d\dot{m}}{dt} = \frac{dpA + \sum(\dot{m}\,u) - 4c_f\,\frac{\rho u|u|}{2}\,\frac{dxA}{D} - K_p\left(\frac{\rho u|u|}{2}\right)A}{dx} \tag{3}$$

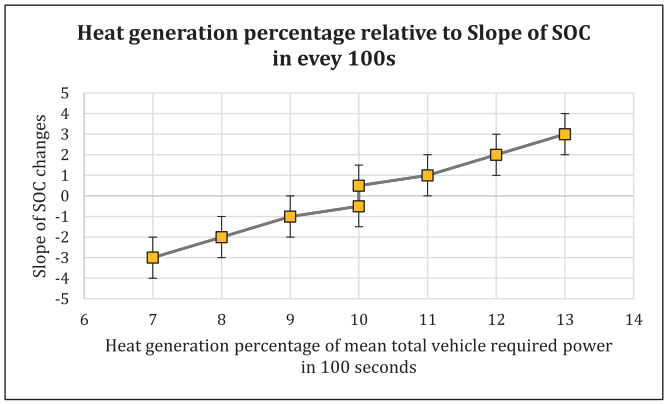

Fig. 3. Heat generation percentage of mean total vehicle required power relative to Slope of SOC change.

Table 2
Compressor, fan, and pump governing equations.

Description	Equation
Fan and compressor Inlet total temperature	$T_{total\ in} = T_{in} + \frac{u_{in}^2}{2C_p}$ (7)
Fan and compressor enthalpy change	$\Delta h_s = C_p T_{total\ in}\left(PR^{\frac{\gamma-1}{\gamma}} - 1\right)$ (8)
Fan and compressor Outlet enthalpy	$h_{in} = h_{in} + \Delta h_s / \eta_s$ (9)
Fan and compressor Power consumption	$P = \dot{m}(h_{out} - h_{in})$ (10)
HC & BC mass flow rate	$\dot{m} = \rho.\eta_v.n.V_D$ (11)

2.2.1. Heat exchanger model

The heat exchanger (HX) is composed of two different parts named master and slave. The master computes the internal heat transfer of HX, and heat transfer between air and the outer surface of the pipe is computed by the slave [46].

Table 1 shows the master and slave fluid flow properties of each three HXs that are implemented in the present simulation. HX governing equation is represented as follow:

$$\frac{dT_{wall}}{dt} = \frac{Q_s + Q_m}{\rho V C_p} = \frac{\left(hA\Delta T - \frac{2kA\Delta T_w}{d}\right)_m + \left(hA\Delta T - \frac{2kA\Delta T_w}{d}\right)_s}{\rho V C_p} \quad (4)$$

2.2.2. Heat generation model

The total heat generation of the battery is mainly composed of reversible heat from electrochemical reactions, irreversible Joule heat, heat from side reactions, and heat of mixing. In the present study, battery heat dissipation is extracted from experiments, and a novel heat generation model is proposed based on the experimental data. The heat generation of the battery is comprehensively studied in previous works for the steady-state charge or discharge of the battery. These models are far from the heat generation in real driving conditions.

Experiments have been conducted to measure the heat generation during real driving conditions of the battery pack. The battery heat generation is computed by Eq. (5).

$$Q = \rho \dot{V} C_p \Delta T \quad (5)$$

$\dot{V}$ is the coolant volume flow rate and is measured by the accurate flow meter. Two thermocouples measure temperature differences at the inlet and outlet of the battery pack. Physical properties are assumed to remain constant throughout the experiment, which is reasonable due to the relatively small temperature range. In the present study, the total heat transfer of the battery pack is computed, and no information is needed about the underlying mechanisms or processes responsible for heat generation in the cells. Notably, the heat loss of the battery pack to the surroundings is not considered due to the insulation of the battery pack.

One of the theoretical models for the heat generation rate of the battery cells is shown in Eq. (6) [47].

$$Q_{\text{theoretical}} = I.(U(1 - SOC) - V) - I.T\frac{\partial U(1 - SOC)}{\partial T} + \mathrm{C_p}\frac{dT}{dt} \quad (6)$$

I the current (positive on discharge), V the cell potential, and U is the open-circuit potential evaluated at the average state of charge in the electrodes. T is the temperature, and Cp is the heat capacity. However, due to relatively small temperature changes, the second term is ignored in the present study [48]. According to Eq. (6), the battery heat generation is expected to be proportional to the SOC variation rate and the product of voltage and amper of the battery(or required power). Our experiments show that the heat generation is proportional to the stored/consumed power of the battery in every 100 s of the cycle. The heat generation is also relative to the slope of SOC at every 100 s.

Fig. 3 shows the battery heat generation as a function of the total required power percentage for the different slopes of SOC. As is shown in this figure, the battery heat generation is 7 to 13% of the mean total vehicle required power in 100 s at the different slopes of SOC in 100 s. In other words, the charge or discharge of the battery is recognized by the slope of SOC. This model represents that the heat generation in discharge (negative slope of SOC) is lower than the battery's charging condition (positive slope of SOC). As can be seen in this figure, for the moderate charge or discharge rate ($-0.5 <$ slope of SOC < 0.5), the generated heat in the battery equals 10% of the required power. Notably, this model is a time averaging model whose implementation is limited to long driving distances (more than 500 s).

In this study, the battery pack is simplified as pipe considering pressure drop and corresponding volume. The generated heat of the battery is modeled with the experiments and imposed directly to the pipe.

2.2.3. Compressor, pump, and fan modeling

The pump and scroll compressor is modeled based on displacement revolution, volumetric efficiency, and isentropic efficiency. The fan is also modeled with an operating map based on volumetric flow rate and pressure. Efficiencies, operating maps, and other data are extracted by standard test or the manual from the supplier. Corresponding correlations are provided in Table 2.

3. Experiments and model validation

3.1. Experimental setup

A plug-in series hybrid electric vehicle is developed and made by Irankhodro Powertrain company and is shown in Fig. 4. Lots of driving tests are defined for the vehicle to evaluate design parameters. To evaluate vehicle energy consumption, different real driving conditions including high traffic jams, steep roads, highways, and different ambient temperatures, are defined in the driving cycles.

The combustion engine is set off for accurate energy consumption measurements in all driving tests. Therefore, vehicle energy is only extracted from the battery. Table 3 demonstrates the BTMS component's specifications in detail. Data transfer between different vehicle modules, including the vehicle control unit (VCU), is conducted on the CAN 500 k network. The messages on the network are updated every 10 or 100 milliseconds based on the importance of transferred data. Data acquisition is performed by ETAS/ES581.4 as the intermediate hardware between the vehicle and computer. Two K-type thermocouples are located upstream and downstream of the battery pack. The flow meter is located after the centrifugal electric pump. A K-type thermocouple also measures the ambient temperature. The battery state of charge (SOC) is extracted through VCU. Instrumentation and uncertainties of experimental devices are shown in Table 4.

Fig. 4. Plugin series hybrid electric vehicle.

Table 3
Specifications of BTMS circuits.

Circuit	Components	Specifications
BC	Electric pump	Rated flow: 4.8 l/min
	Radiator	Type: tube & fin
		Number of row of tubes: 10
		Max heat transfer: 1.2 kW
HC	Scroll compressor	Displacement: 27 cc/r
		Range of speed: 1000–6500 RPM
		Power input: 0.35–2.1 kW
	Chiller	Type: Brazed Plate
		Number of Plates: 22
		Max heat transfer: 3.9 kW
	Condenser	Type: tube & fin
		Number of row of tubes: 33
		Max heat transfer: 14.3 kW
	Cooling fan	Range of speed: 0–5000 RPM
		Mass flow rate: 0–2.9 m^3/s

Table 4
Accuracy and uncertainty of experimental facilities.

Parameters	Instruments	Range	Uncertainty
Coolant Temperature(°C)	K-type thermocouple	0–1000	±2
Ambient temperature(°C)	K-type thermocouple	0–1000	±2
Pressure (bar)	Pressure transducer	0–4	±0.05
Mass flow rate(L/min)	Magnetic flow meter	0–20	2%
Battery power input/output (kW)	Electric power meter	0–100	±0.2%
SOC	VCU	0–100	±3%

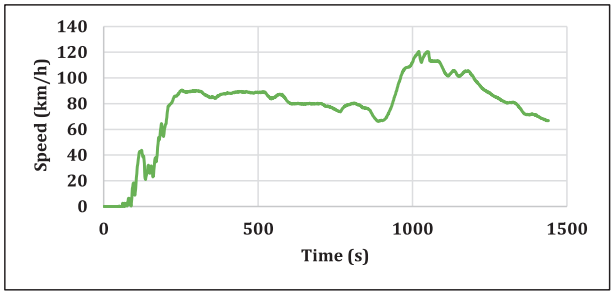

Fig. 5. Driving cycle during the experiment.

3.2. Model validation

Average heat generation at every 100 s is calculated based on the slope of SOC and the required power of the vehicle. This heat source is imposed on the model, and the inlet and outlet temperature of the battery pack is calculated. The driving cycle of the experiment is shown in Fig. 5.

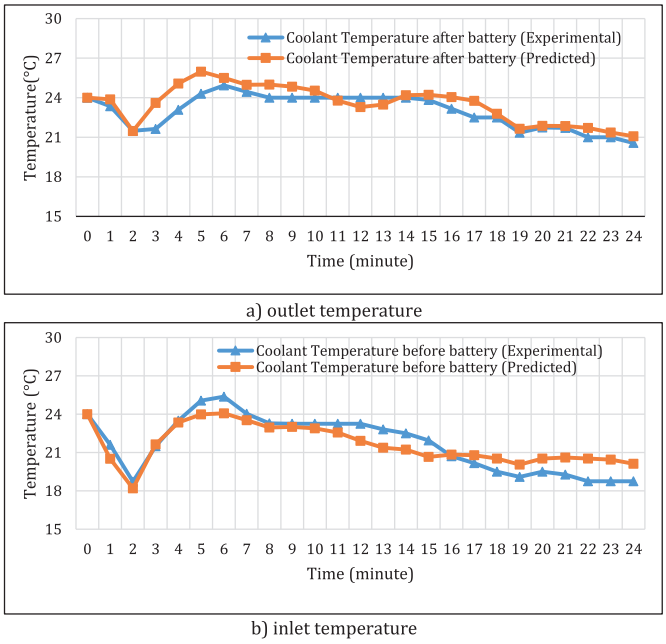

Fig. 6. Battery pack outlet and inlet temperature.
a) outlet temperature, b) inlet temperature.

The battery pack's predicted and measured inlet and outlet coolant temperature are compared with experimental data in Fig. 6. As are shown in this figure, there is a good agreement between the experimental and predicted temperatures. The predicted temperature follows the trend of measured data very well. The presented model is a time-averaging model that is not sensitive to rapid fluctuations. Therefore, the rapid fluctuations cannot be seen in the model. Notably, some simplifications, such as insulated surroundings, do not exactly exist in the experiments. Thus, some differences between measured and predicted are expected.

4. BTMS optimization methodology

4.1. Optimization process

In the present study, the total cost of ownership (TCO) is considered the objective function to optimize the initial and operational cost of BTMS. A genetic algorithm, especially NSGA III, is implemented to minimize TCO by considering cost-effective variables. The initial random population with 20 different configurations is generated first. The objective function is evaluated for all of these 20 configurations. The population is updated based on mutation, crossover, and other genetic algorithm functions at each iteration. The operative functions of the

Table 5
Independent variables and constraints.

Parameters	Range
Chiller HXM	0.9–10
Condenser HXM	0.7–1.5
Radiator HXM	0.7–1.5
Compressor speed	1000–6500
Fan speed	1000–5000
Battery pack inlet temperature	18–26

genetic algorithm continually improve the population quality by prioritizing the configurations with the minimum TCO. This procedure is converged until no improvement is observed in the population.

Direct and indirect costs of BTMS for a series hybrid electric vehicle, including initial and operational costs, are considered to be optimized. The intended objective function is the summation of fuel consumption cost for BTMS operation in 5 years with taking into account interest rate and initial costs of components. The vehicle's estimated mileage of five years is 100,000 km. The monthly mileage by vehicle in each month is assumed to be the same. The interest rate is set to 4%. All expenses are computed by the US dollar. The objective function can be expressed as follow:

$$TCO = Z + X \tag{12}$$

$$Z = S\left[\frac{(1+i/m)^{mn}-1}{i/m(1+i/m)^{mn}}\right] \tag{13}$$

Z is the 5-year fuel cost, X is the initial cost of components, i is the interest rate, m is the number of months, and n is the year. The operating cost is calculated based on the amount of fuel required to generate enough power for the BTMS. Fuel consumption is derived as follow:

$$power\ consumption = \int_{t=0}^{t=t_{cycle}} (power\ consumption\ of\ compressor\&fan)\ dt \tag{14}$$

$$Fuel\ consumption = \text{power generation density}\left[\frac{gram}{kW \bullet h}\right] \times power\ consumption[kW \bullet h] \tag{15}$$

The specific fuel consumption of engine is considered 225[gram/(kWh)]. Considering the 90% efficiency for mechanical and electrical losses of the generator, the electric power is produced with a 250 [gram/

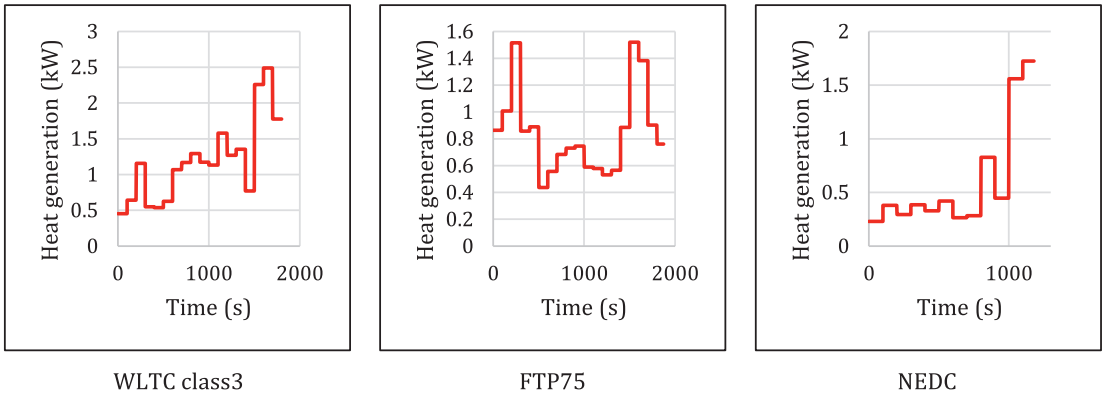

Fig. 7. Battery heat generation during driving cycles.

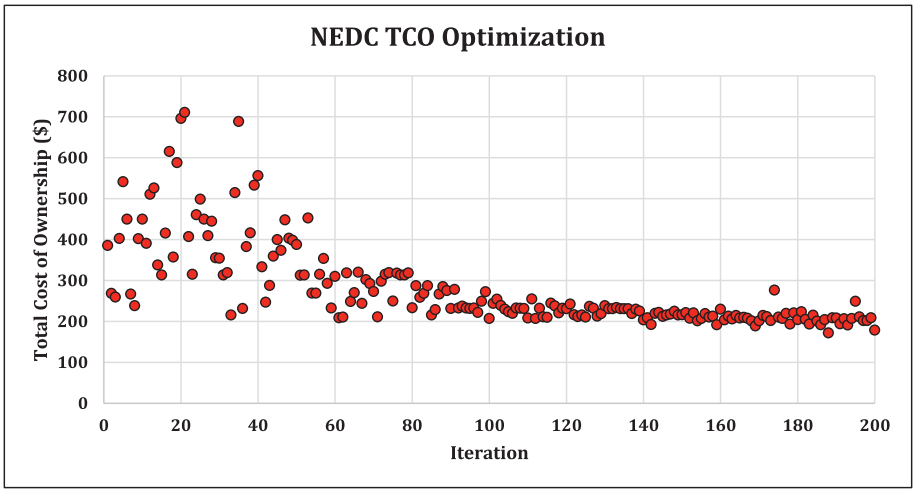

Fig. 8. Single objective optimization of BTMS over generations with respect to TCO in NEDC.

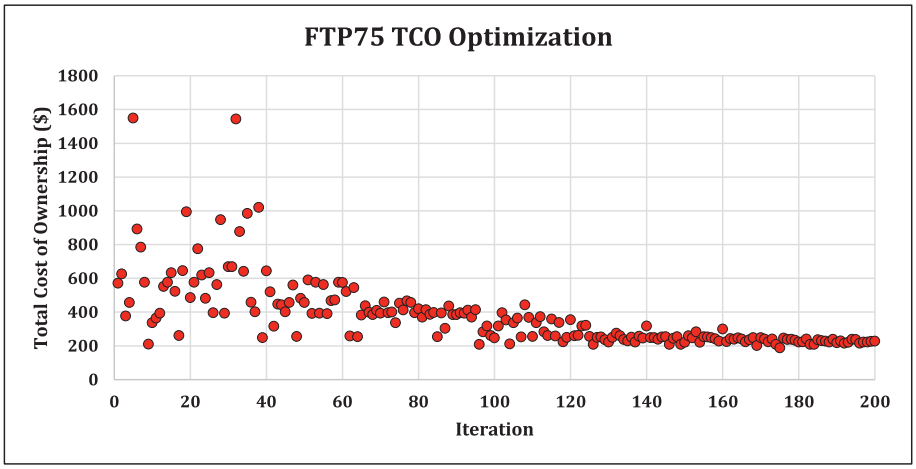

Fig. 9. Single objective optimization of BTMS over generations with respect to TCO in FTP75.

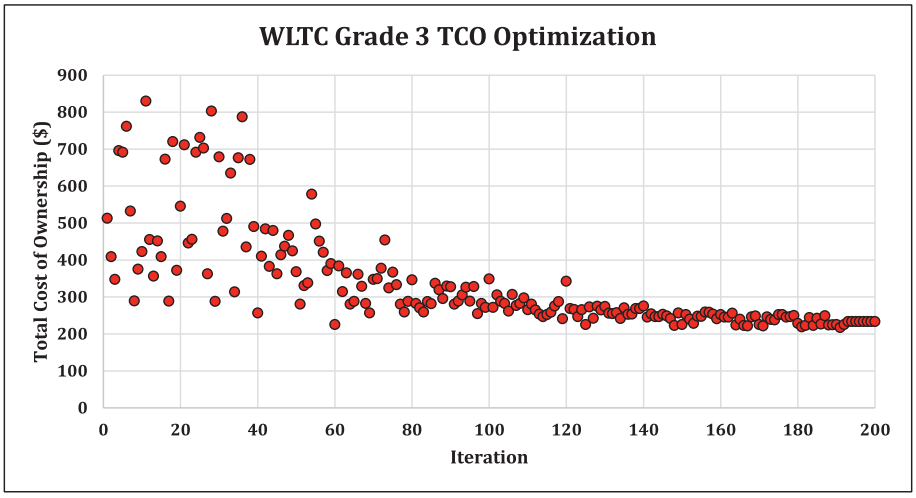

Fig. 10. Single objective optimization of BTMS over generations with respect to TCO in WLTC3.

Table 6
Initial Values of independent variables in TCO optimization.

Device corresponding parameter	Initial value
Radiator HXM	1
Chiller HXM	1
Condenser HXM	1
Compressor Speed	2000 rpm
Fan Speed	2000 rpm

(kWh)] efficiency. The fuel price is considered 0.8 US dollars per liter.

The chiller's and condenser's size, the compressor's speed, and the fan are considered the independent variables. To consider the effects of condenser and chiller size, heat exchanger multipliers (HXMs) are defined for these devices. The heat transfer area of the condenser and chiller are multiplied by these coefficients. The variation in the initial cost of these two components is calculated by multiplying the initial cost into one-tenth of the multiplier minus one. The initial cost of the radiator, chiller, and condenser are 20$, 60$, and 15$ for multiplier 1.0, respectively. The limitation associated with variables and constraints is shown in Table 5.

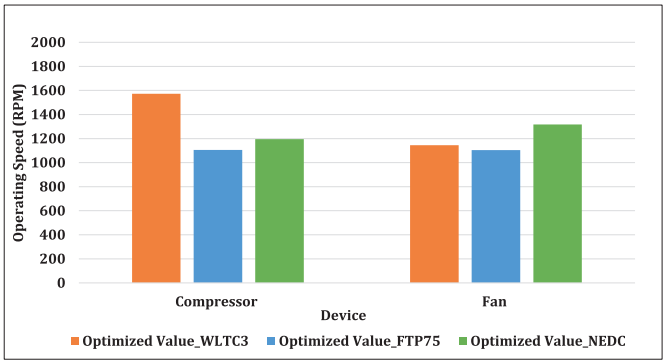

Fig. 11. Optimized operating speed of compressor and fan with respect to different driving cycles.

4.2. Optimization verification

In order to verify the optimization method, the optimization process is implemented in a similar cost optimization study [49]. The results revealed that the timed average cost for different batteries' maximum capacity is 0.148526, 0.013141, and 0.000412 $/hr for three batteries' maximum power of 100, 150,200 kW, respectively. The extracted results

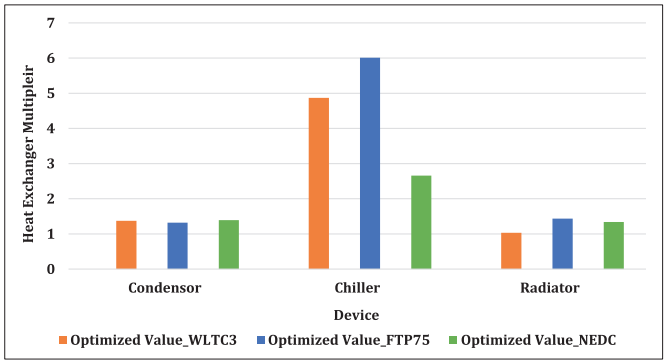

Fig. 12. Optimized HXMs of condenser, chiller, and radiator with respect to different driving cycles.

are in good agreement with identical solutions in the literature [49].

5. Results and discussions

To optimize the current BTMS of the vehicle, the total cost of ownership is minimized in three different standard driving cycles. NEDC, FTP75, and WLTC class 3 are considered in the present study to optimize BTMS and investigate the effects of different driving conditions on the optimized arrangement. The heat generation of the battery during different driving cycles is shown in Fig. 7. This figure shows that the highest peak in heat generation is related to the WLTC cycle. The heat generation during the WLTC is also higher than the other cycles. In FTP75, there are two heat generation peaks at the beginning and end of the cycle. So, BTMS should only overcome these two regions, and heat generation is relatively low during the rest of the cycle. The heat generation during the NEDC is the least amount compared to the other cycles. There is a peak in the heat generation of the NEDC cycle that is related to the suburban driving conditions. The battery cell temperature is proportional to the battery coolant temperature. Thus, the battery coolant temperature should be controlled in the appropriate range by the BTMS. The TMS of the present study shown in Fig. 2 controls the coolant temperature in the range of 16–28°C.

The optimization trends for the NEDC, FTP75, and WLTC3 cycles are shown in Figs. 8 to 10, respectively. The population size is 20 and the mutation index is set to 0.2. During the optimization process, the independent variables are varied according to the TMS control strategy to determines the coolant passage (to the chiller or the radiator) under various situations. The objective function is considered the total cost of ownership for five years. These figures show that TCO is converged to around 200$ for all driving cycles. This shows that this minimum is independent of the driving cycle and driving behavior. The larger chiller is needed for the accelerated or suburban driving conditions to dissipate the generated heat. This increases the initial cost of ownership. For the bigger chiller size, the compressor speed decreases to moderate the cooling rate in the chiller path. Therefore, the operating cost is decreased at this condition due to the lower compressor speed. Consequently, the TCO is converged to the fixed value for different driving

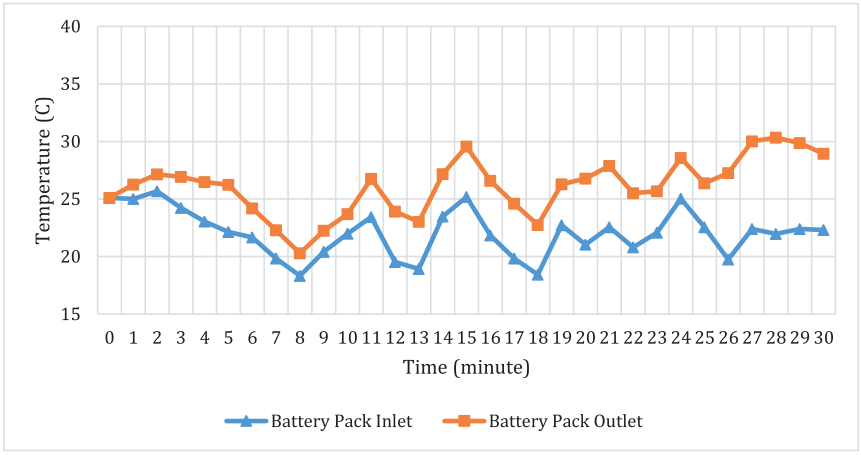

a) temperature in non-optimized system

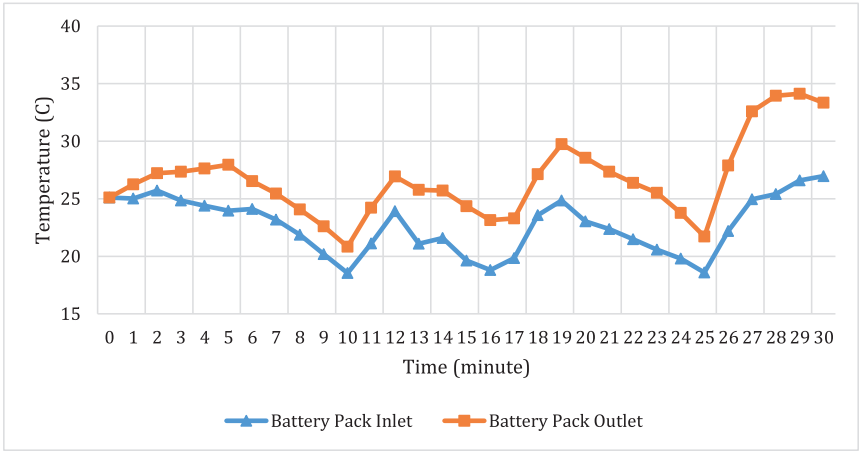

b) temperature in optimized system

Fig. 13. Temperature variations of battery coolant during WLTC class 3 driving cycle.
a) temperature in non-optimized system, b) temperature in optimized system.

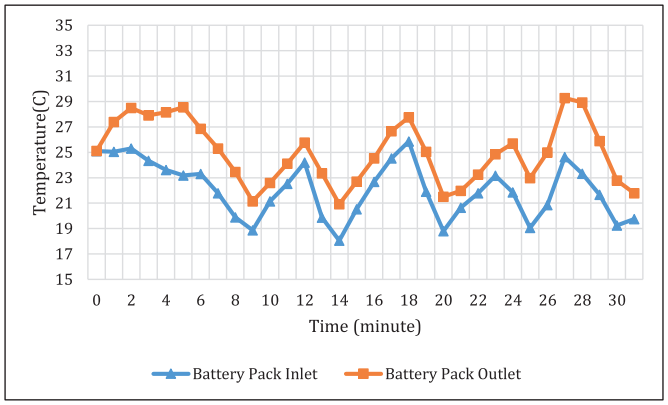

a) temperature in non-optimized system

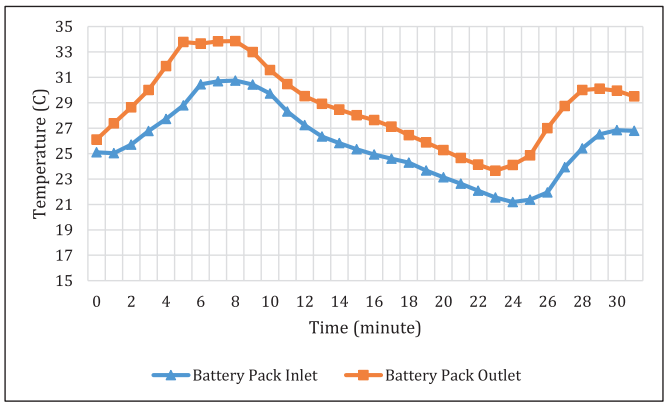

b) temperature in optimized system

Fig. 14. Temperature variations of battery coolant during FTP 75 driving cycle. a) temperature in non-optimized system, b) temperature in optimized system.

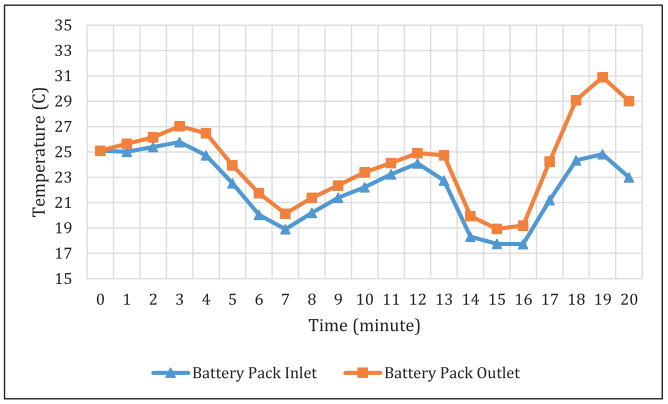

a) temperature in non-optimized system

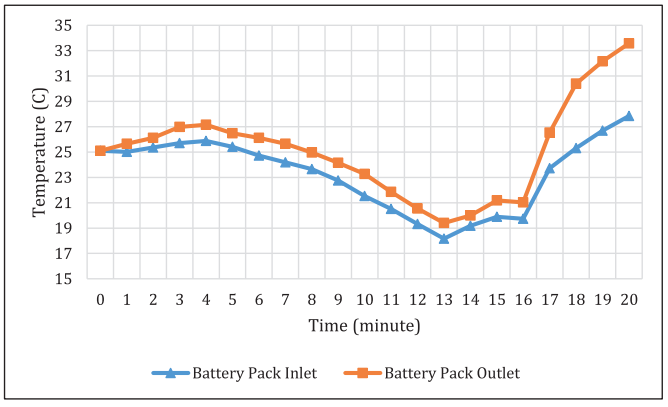

b) temperature in optimized system

Fig. 15. Temperature variations of battery coolant during NEDC driving cycle. a) temperature in non-optimized system, b) temperature in optimized system.

conditions and heat exchanger sizes. These figures also emphasize that the operating costs of BTMS for five years are comparable with the initial cost of heat exchangers. This shows the importance of optimization of operating costs during vehicle lifecycle.

The initial values of independent variables of BTMS are shown in Table 6. As shown in this table, the initial speed of compressor and fan are set to 2000 rpm. The multipliers of heat exchangers are also set to unity.

All of the HXMs along with the compressor and fan speeds, are optimized to reduce the total cost of ownership by considering the constraints of battery temperature. The Thermal management strategy is according to Fig. 2. The optimized values of independent variables are presented in Figs. 11 and 12. As shown in these figures, the compressor and fan's speed is decreased compared to the initial value. Meanwhile, the chiller size is increased in the optimized solution for all driving cycles. It is also notable that the size of the condenser and radiator are not significantly changed during optimization. This is due to the limitations of HXMs for radiator and condenser that are limited by the packaging constraints of these heat exchangers. As previously mentioned, the optimum configuration of BTMS does not considerably vary for different driving cycles. Therefore, one of the optimum configurations can be considered for the overall optimum of BTMS. The only exception in this regard is related to the size of the chiller for the NEDC driving cycle. The optimum chiller size in the NEDC driving cycle is approximately half of other driving cycles. This is due to the moderate driving behavior during the NEDC that leads to less heat dissipation by the battery. These figures also emphasize the importance of the chiller path for optimum energy consumption. As shown in this figure, the compressor's speed and the size of the chiller are more sensitive to the driving conditions than the other variables

Fig. 13 shows the battery coolant temperature variations during the WLTC driving cycle for the base and optimized BTMS. The compressor is turned on at each peak of battery coolant temperature and is turned off at each minimum. As shown in this figure, the temperature variations are decreased for the optimized BTMS due to improved chiller heat transfer capacity. Fluctuations of battery coolant temperature are also inappropriate for the battery cell and decrease its lifetime. The compressor frequency on/off is also decreased in the optimized arrangement. This side effect improves the compressor lifetime and decreases the energy consumption in real driving conditions.

Fig. 14 shows the temperature variations of battery coolant during the FTP75 driving cycle for the initial and optimized BTMS. This figure shows that significant improvement can be seen in the temperature fluctuations. As previously shown in Fig. 12, the most heat transfer capacity of the chiller is related to the optimized BTMS at the FTP75 driving cycle. This clearly shows that the size of the chiller influences directly on the temperature fluctuations of the battery coolant. The main limitation for the greater chiller in the optimization is the initial cost. The initial price of the chiller increases with its size directly. It is also notable that the larger chiller leads to rapid cooling that increases the frequency of the compressor on/off in moderate driving conditions.

The temperature fluctuations of battery coolant during the NEDC cycle are shown in Fig. 15. Due to the moderate driving conditions in this cycle, the temperature oscillations are not as much as other driving cycles. Therefore, as previously shown in Fig. 12, the minimum chiller size is related to the NEDC driving cycle. As can be seen in these figures, the optimization is tried to converge the chiller size and the compressor speed to the appropriate conditions that reduce the temperature variations into one peak and one minimum. This moderate cooling maintains the coolant temperature in the suitable range and decreases the

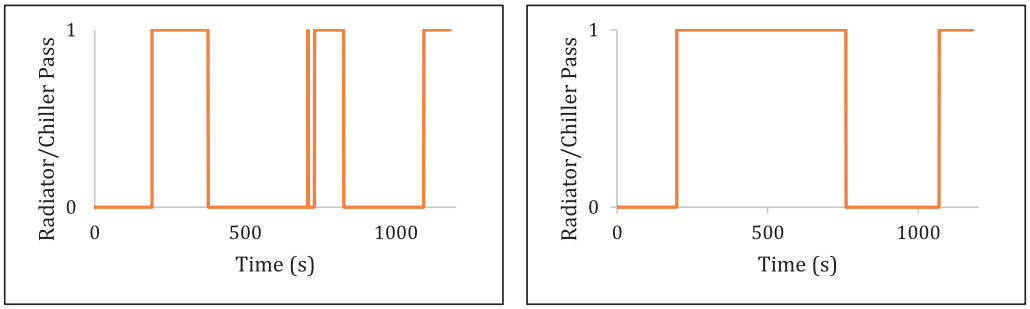

Fig. 16. Cooling Passage of optimized and non-optimized system during NEDC driving cycle, 0 represents radiator pass, 1 represents Chiller pass.

temperature fluctuations. This goal cannot be met in aggressive driving conditions with high acceleration and decelerations due to the low energy recovery during decelerations.

Fig. 16 represents the cooling passage (radiator or chiller) of BTMS during the NEDC driving cycle. As shown in this figure, the frequency of changing passage decreases after optimization. Thanks to the bigger chiller size in the optimized BTMS, the compressor works at a slower speed than the base BTMS. Therefore, the heat transfer rate is decreased in the optimized chiller passage. In this way, the reduction of coolant temperature in the chiller passage is moderate, and the chiller passage will be active for a longer time. This improvement decreases the temperature fluctuations during driving and minimizes energy consumption. This reduction frequency also improves the compressor lifecycle and battery cell health. This trend also can be seen in other driving cycles.

6. Conclusions

In the present study, the BTMS of a hybrid electric vehicle is modeled and optimized to minimize the total cost of ownership during five years. A novel heat generation model is proposed based on the real driving conditions. This model is implemented in the GT-suite and is validated with the experimental data. Three different standard driving cycles are investigated for optimization. The conclusions are as follows:

- According to the experiments, it is found that the battery heat generation is proportional to the stored/consumed power of the battery in every 100 s of the cycle. The heat generation is also relative to the slope of SOC at every 100 s.
- The speed of the compressor and fan is decreased in the optimized BTMS for all driving conditions. Meanwhile, the chiller size is increased in the optimized solution for all driving cycles. It is also notable that the size of the condenser and radiator are not significantly changed during optimization. The optimum configuration of BTMS does not considerably vary for different driving cycles. Therefore, one of the optimum configurations can be considered for the overall optimum TCO of BTMS.
- Due to the bigger chiller size in the optimized BTMS, the compressor works at a slower speed than the base BTMS. Therefore, the heat transfer rate is decreased in the optimized chiller passage. In this way, the reduction of coolant temperature in the chiller passage is moderate, and the chiller passage will be active for a longer time. This improvement decreases the temperature fluctuations during driving and minimizes energy consumption.
- The total cost of ownership is converged to 200 dollars for all driving conditions.
- The temperature variations are decreased for the optimized BTMS due to chiller heat transfer capacity that reduces the compressor speed.
- The most sensitive independent variable to the optimization is the chiller size and the compressor speed. The optimization is tried to converge the chiller size and the compressor speed to the appropriate conditions that reduce the temperature variations into one peak and one minimum. This moderate cooling maintains the coolant temperature in the suitable range and decreases the temperature fluctuations.

Author statement

Ali Asef: Conceptualization, Methodology, Experiments,Writing-Original draft preparation **Iman Chitsaz.**: Supervision, Writing-Reviewing and Editing, **Navid Madani**: Technical supervision, Experiments.

Declaration of competing interest

The authors declare that they have no known competing financial interests or personal relationships that could have appeared to influence the work reported in this paper.

Acknowledgments

The authors would like to express special thanks to the Irankhodro powertrain company for their support in the experimental tests.

References

[1] A.K. Thakur, et al., A state of art review and future viewpoint on advance cooling techniques for lithium–ion battery system of electric vehicles, J.Energy Storage 32 (2020), 101771.
[2] X. Hao, et al., Range cost-effectiveness of plug-in electric vehicle for heterogeneous consumers: an expanded total ownership cost approach, Appl. Energy 275 (2020), 115394.
[3] L. Lander, et al., Cost and carbon footprint reduction of electric vehicle lithium-ion batteries through efficient thermal management, Appl. Energy 289 (2021), 116737.
[4] S. Kumar, R. Udaykumar, Stochastic model of electric vehicle parking lot occupancy in vehicle-to-grid (V2G), Energy Procedia 90 (2016) 655–659.
[5] F. Wang, Y. Deng, C. Yuan, Life cycle assessment of lithium oxygen battery for electric vehicles, J. Clean. Prod. 264 (2020), 121339.
[6] S. Alshahrani, M. Khalid, M. Almuhaini, Electric vehicles beyond energy storage and modern power networks: challenges and applications, IEEE Access 7 (2019) 99031–99064.
[7] M. Hannan, et al., Review of energy storage systems for electric vehicle applications: issues and challenges, Renew. Sustain. Energy Rev. 69 (2017) 771–789.
[8] Q. Wang, et al., A critical review of thermal management models and solutions of lithium-ion batteries for the development of pure electric vehicles, Renew. Sustain. Energy Rev. 64 (2016) 106–128.
[9] Y. Gan, et al., A numerical study on the performance of a thermal management system for a battery pack with cylindrical cells based on heat pipes, Appl. Therm. Eng. 179 (2020), 115740.
[10] Z. Rao, et al., Experimental investigation of battery thermal management system for electric vehicle based on paraffin/copper foam, J. Energy Inst. 88 (3) (2015) 241–246.
[11] M. Malik, et al., Experimental investigation of a new passive thermal management system for a li-ion battery pack using phase change composite material, Electrochim. Acta 257 (2017) 345–355.

[12] M.M. Heyhat, S. Mousavi, M. Siavashi, Battery thermal management with thermal energy storage composites of PCM, metal foam, fin and nanoparticle, J.Energy Storage 28 (2020), 101235.
[13] Y. Gan, et al., Development of thermal equivalent circuit model of heat pipe-based thermal management system for a battery module with cylindrical cells, Appl. Therm. Eng. 164 (2020), 114523.
[14] G.-H. Kim, A. Pesaran, Battery thermal management design modeling, World Electr.Veh.J. 1 (1) (2007) 126–133.
[15] W. Wu, et al., A critical review of battery thermal performance and liquid based battery thermal management, Energy Convers. Manag. 182 (2019) 262–281.
[16] X. Tang, et al., Performance analysis on liquid-cooled battery thermal management for electric vehicles based on machine learning, J. Power Sources 494 (2021), 229727.
[17] X. Kuang, et al., Research on control strategy for a battery thermal management system for electric vehicles based on secondary loop cooling, IEEE Access 8 (2020) 73475–73493.
[18] Z. Tian, et al., Performance evaluation of an electric vehicle thermal management system with waste heat recovery, Appl. Therm. Eng. 169 (2020), 114976.
[19] Z. Tian, et al., Investigation on an integrated thermal management system with battery cooling and motor waste heat recovery for electric vehicle, Appl. Therm. Eng. 136 (2018) 16–27.
[20] Y.M. Alkhulaifi, N.A. Qasem, S.M. Zubair, Improving the performance of thermal management system for electric and hybrid electric vehicles by adding an ejector, Energy Convers. Manag. 201 (2019), 112133.
[21] H. Hamut, I. Dincer, G. Naterer, Exergy analysis of a TMS (thermal management system) for range-extended EVs (electric vehicles), Energy 46 (1) (2012) 117–125.
[22] H. Hamut, I. Dincer, G. Naterer, Analysis and optimization of hybrid electric vehicle thermal management systems, J. Power Sources 247 (2014) 643–654.
[23] X. Wang, et al., Surrogate based multidisciplinary design optimization of lithium-ion battery thermal management system in electric vehicles, Struct. Multidiscip. Optim. 56 (6) (2017) 1555–1570.
[24] X. Wang, et al., Multidisciplinary and multifidelity design optimization of electric vehicle battery thermal management system, J. Mech. Des. 140 (9) (2018).
[25] M. Yao, et al., Performance simulation of a heat pipe and refrigerant-based lithium-ion battery thermal management system coupled with electric vehicle air-conditioning, Appl. Therm. Eng. 191 (2021), 116878.
[26] A.A.H. Akinlabi, D. Solyali, Configuration, design, and optimization of air-cooled battery thermal management system for electric vehicles: a review, Renew. Sustain. Energy Rev. 125 (2020), 109815.
[27] H. Fayaz, et al., Optimization of thermal and structural design in lithium-ion batteries to obtain energy efficient battery thermal management system (BTMS): a critical review, Arch.Comput.MethodsEng. 29 (2021) 129–194.
[28] J. Liang, Y. Gan, Y. Li, Investigation on the thermal performance of a battery thermal management system using heat pipe under different ambient temperatures, Energy Convers. Manag. 155 (2018) 1–9.
[29] Y. Liu, J. Zhang, Design a J-type air-based battery thermal management system through surrogate-based optimization, Appl. Energy 252 (2019), 113426.
[30] N. Wang, et al., Heat dissipation optimization for a serpentine liquid cooling battery thermal management system: an application of surrogate assisted approach, J.Energy Storage 40 (2021), 102771.
[31] J. Weng, et al., Optimization of the detailed factors in a phase-change-material module for battery thermal management, Int. J. Heat Mass Transf. 138 (2019) 126–134.
[32] J. Weng, et al., Optimization of the internal fin in a phase-change-material module for battery thermal management, Appl. Therm. Eng. 167 (2020), 114698.
[33] J. Cen, Z. Li, F. Jiang, Experimental investigation on using the electric vehicle air conditioning system for lithium-ion battery thermal management, EnergySustain. Dev. 45 (2018) 88–95.
[34] K. Chen, et al., Configuration optimization of battery pack in parallel air-cooled battery thermal management system using an optimization strategy, Appl. Therm. Eng. 123 (2017) 177–186.
[35] K. Chen, et al., Structure optimization of parallel air-cooled battery thermal management system, Int. J. Heat Mass Transf. 111 (2017) 943–952.
[36] K. Chen, et al., Structure optimization of parallel air-cooled battery thermal management system with U-type flow for cooling efficiency improvement, Energy 145 (2018) 603–613.
[37] L. Cheng, et al., Surrogate based multiobjective design optimization of lithium-ion battery air-cooled system in electric vehicles, J.Energy Storage 31 (2020), 101645.
[38] Y. Shi, et al., Optimization of air-cooling technology for LiFePO4 battery pack based on deep learning, J. Power Sources 497 (2021), 229894.
[39] M. Shen, Q. Gao, System simulation on refrigerant-based battery thermal management technology for electric vehicles, Energy Convers. Manag. 203 (2020), 112176.
[40] Y. Fan, et al., Optimization of cooling strategies for an electric vehicle in high-temperature environment, Appl. Therm. Eng. 195 (2021), 117088.
[41] J. Hou, et al., A direct optimization strategy based on field synergy equation for efficient design of battery thermal management system, Int. J. Heat Mass Transf. 184 (2022), 122304.
[42] M. Lu, et al., Research progress on power battery cooling technology for electric vehicles, J.Energy Storage 27 (2020), 101155.
[43] N. Javani, et al., Exergy analysis and optimization of a thermal management system with phase change material for hybrid electric vehicles, Appl. Therm. Eng. 64 (1–2) (2014) 471–482.
[44] Y. Li, et al., Optimization of thermal management system for Li-ion batteries using phase change material, Appl. Therm. Eng. 131 (2018) 766–778.
[45] . Technologies, G. GT-Suite Flow Theory Manual.
[46] G.R. P Dinakar, Modelling and Simulation of Cooling Systems for BEV High Voltage Battery, in Department of Applied Mechanics, Chalmers University of Technology, 2016.
[47] K.E. Thomas, J. Newman, Heats of mixing and of entropy in porous insertion electrodes, J. Power Sources 119–121 (2003) 844–849.
[48] K.E. Thomas, J. Newman, Heats of mixing and of entropy in porous insertion electrodes, J. Power Sources 119 (2003) 844–849.
[49] G.A. Mary, R. Rajarajeswari, Smart grid cost optimization using genetic algorithm, Int. J. Res. Eng. Technol. 3 (07) (2014) 282–287.